Theoretical study of the reaction 2,5-dimethylfuran + H → products

Baptiste Sirjean, René Fournet

Theoretical study of the reaction 2,5-dimethylfuran + H → products

Baptiste Sirjean and René Fournet

Laboratoire Réactions et Génie des Procédés, CNRS, Université de Lorraine, ENSIC,

1 rue Grandville BP 20451 54001 Nancy Cedex, France

Corresponding Author:

B. Sirjean

Laboratoire Réactions et Génie des Procédés

CNRS, Nancy Université,

1 rue Grandville BP 20451 54001 Nancy Cedex, France

Phone: +3338-317-5202

Fax: +3338-332-2975

Email: baptiste.sirjean@univ-lorraine.fr

Colloquium Topic Area: Reaction Kinetics

Total length: 6056 words
Main text: 3755 words (MSWord 2007 word count)
References: (22 references + 2) x (2.3 lines/reference) x (7.6 words/line) = 419 words
Table 1: (5 lines + 2 lines) x (7.6 words/line) x 1 column = 53 words
Table 2: (20 lines + 2 lines) x (7.6 words/line) x 2 columns = 182 words
Table captions: 25 words
Tables (total): 260
Figure 1: [53 mm + 10 mm] x 2.2 words/mm x 1 column = 139 words
Figure 2: [54 mm + 10 mm] x 2.2 words/mm x 1 column + 9 = 150 words
Figure 3: [65 mm + 10 mm] x 2.2 words/mm x 1 column = 165 words
Figure 4: [55 mm + 10 mm] x 2.2 words/mm x 1 column = 143 words
Figure 5: [52 mm + 10 mm] x 2.2 words/mm x 1 column = 136 words
Figure 6: [79 mm + 10 mm] x 2.2 words/mm x 2 columns = 396 words
Figure 7: [52 mm + 10 mm] x 2.2 words/mm x 1 column = 136 words
Figure 8: [56 mm + 10 mm] x 2.2 words/mm x 1 column = 145 words
Figure captions: 212
Figure (total): 1622

Submitted for consideration at the 34th International Symposium on Combustion, Warsaw University of Technology, Poland, July 29 - August 3, 2012

Theoretical study of the reaction 2,5-dimethylfuran + H → products

Baptiste Sirjean and René Fournet

Laboratoire Réactions et Génie des Procédés, CNRS, Nancy Université, ENSIC,

1 rue Grandville BP 20451 54001 Nancy Cedex, France

Abstract

The reaction of 2,5-dimethylfuran (DMF) with H-atoms was studied using a potential energy surface calculated at the CBS-QB3 level of theory and master equation/RRKM modeling. Hydrogen abstraction by H-atom and hydrogen additions on DMF were considered. As the decomposition pathways of the initial adducts were unknown, a large number of decomposition routes was explored for these adducts. An important number of interconnected product channels was found and preliminary master equation calculations were performed to select the crucial wells and exit channels. The ipso substitution DMF + H→ methylfuran (MF) + CH_3 and the formation of 1,3-butadiene and acetyl radical (CH_3CO) were found to be the major product channels in the addition process. The total calculated rate constant was found in good agreement with experimental data and is nearly pressure-independent. A small sensitivity to pressure was found for the computed branching ratios. At 1 bar, the yields of the two product channels of the addition process are maximal at 1100 K with computed branching ratios of 39% (MF + CH_3) and 27% (1,3-C_4H_6 + CH_3CO). Above 1300 K, hydrogen abstraction by H-atom becomes dominant and reaches a branching ratio of 56% at 2000 K.

Keywords:

2,5-dimethylfuran; hydrogen-addition; kinetics; quantum chemistry; biofuel

1. Introduction

2,5-dimethylfuran (DMF) is one of the potential liquid fuel produced from biomass with physical properties that make it a promising biofuel. Three advantages over ethanol are usually emphasized (a) its energy density (30MJ/L) is 40% higher than ethanol (21.3 MJ/L) and close to that of gasoline (31.6 MJ/L), (b) DMF boiling point (366.5 K) is higher than ethanol (351.6 K) and is therefore less volatile and (c) DMF is not soluble in water [1]. Recent breakthroughs in the production methods of DMF via catalytic routes are particularly remarkable [2-3]. Consequently, several studies using DMF as a fuel have recently been published. Combustion of DMF was studied in direct-injection spark-ignition engine and the authors observed performances and emissions similar with that of gasoline and ethanol [4-5]. Tian et al. showed that DMF laminar burning velocities are close to that of gasoline [6]. Wu et al. [7] also measured laminar burning velocities of DMF at elevated pressures and discussed flame instabilities. However, detailed combustion chemistry of DMF remains almost totally unknown [8].

Grela et al. [9] studied the unimolecular decomposition of DMF using very low pressure pyrolysis experiments. For temperatures ranging between 1050 and 1270 K and at a pressure of 1 mtorr, they detected two products channels leading to a linear C_6H_6+H_2O, and a linear C_5H_8+CO. They proposed a rearrangement via a cyclopropenylcarbonyl to 2,4-dimethylfuran intermediate followed by a biradicalar ring opening to explain their experimental results. Lifshitz et al. [10] studied the thermal decomposition of DMF in shock tube between 1080 and 1350 K at pressures around 2 bar. They reported decomposition products profiles as a function of temperatures and proposed a reaction mechanism containing 50 species and 180 reactions with a fair number of global and speculative reactions with estimated thermochemical and kinetic parameters fitted to reproduce the experimental products distribution. They considered seven reactions for the DMF+H system. H-abstraction from DMF by H-atoms, leading to the stabilized 5-methyl-2-furanylmethyl (C_6H_7O) radical, were taken into

account with an estimated rate constant of $1.0\times10^{14}\exp(-4026/T)$ $cm^3mol^{-1}s^{-1}$. They also considered six reactions with H-atom grouped in a reaction class called "dissociative attachments":

$$DMF+H\bullet \rightarrow 1,3\text{-butadiene}+CH_3CO\bullet \quad (R1)$$

$$\rightarrow 2\text{-butyne}+CH_3CO\bullet \quad (R2)$$

$$\rightarrow 1,2\text{-butadiene}+CH_3CO\bullet \quad (R3)$$

$$\rightarrow 1\text{-butyne}+CH_3CO\bullet \quad (R4)$$

$$\rightarrow 2\text{-methylfuran (MF)}+CH_3\bullet \quad (R5)$$

$$\rightarrow C_3H_5\bullet+C_2H_4+CO \quad (R6)$$

From an elementary point of view, reactions R1 to R6 are essentially global reactions that could be rationalized by considering the formation of a chemically activated C_6H_9O adduct that further decomposes to products. Reactions R1 to R4 were proposed by Lifshitz et al. to partially account for the four C_4H_6 isomers quantified. Reaction R5 is a classical ipso substitution and (R6) constitutes, in their simulations, the most sensitive reaction for the production of C_2H_4 at 1100 K. All associated rate parameters were estimated by the authors. Wu et al. [11] identified combustion intermediates in a low-pressure premixed laminar DMF/oxygen/argon flame with tunable synchrotron photoionization. They detected more than 70 species and speculated several mechanistic pathways to explain the formation of most of the observed compounds. They showed the presence of C_6H_7O radical, obtained by H-abstractions / initial C-H bond scission from DMF. Recently, Simmie and Metcalfe [12] studied the initial steps in the thermal decomposition of DMF with electronic structure calculations. They explored several pathways and proposed rate coefficients for H-abstraction by H-atom and ipso substitution R5. They showed that H-abstractions from the ring can be neglected up to 2000 K. They also proposed high-pressure rate constants, based on G3 calculations, for the addition of a H-atom on the ring. Hydrogen can add on the carbon atoms linked to methyl groups or on other carbons leading to either $R1C_6H_9O$ or $R2C_6H_9O$ radicals (Figure 1). They explored only one exit channel for each adduct: $R1C_6H_9O$ ⇆

MF+CH_3• and R2C_6H_9O ⇆ C_6H_8O+H•. Friese et al. [13] reported the first experimental measures of the DMF+H rate constant obtained behind reflected shock waves between 980 and 1250 K at pressures of 1.6 and 4.7 bar. They used resonance absorption spectrometry to get time-resolved profiles of hydrogen atoms in the reaction DMF+H → products. They satisfactorily simulated their experimental profiles with a small mechanism containing three reactions: DMF+H → products, DMF → C_6H_7O+H and the decomposition of their H-atom precursor C_2H_5I.

This investigation aims to thoroughly explore the potential energy surface of the DMF+H products reaction by means of high-level quantum chemistry calculations. As almost no information is available in the literature, we explored every possible, yet reasonable, decomposition pathways. From the relevant PES obtained, we determined pressure dependent rate coefficients from master equation/RRKM modeling. Theoretical results are then discussed and compared to Friese et al. experiments.

2. Computational details

Potential energy surfaces were calculated using Gaussian 09 [14] for all stationary and critical structures, using the composite CBS-QB3 method [15]. Analysis of vibrational frequencies confirmed that all transition structures have one imaginary frequency. For a molecule or a radical that can be properly described by a single reference wave function an accuracy of ~1.5 kcal mol^{-1} on the PES can be expected. For comparisons, G4 calculations [16] were also performed for the most important channels. Currently, the G4 version is the most accurate of the popular "G methods" but is also the most computationally expensive. Enthalpies of formation at 298 K were calculated from isodesmic reactions.

Rate coefficients were calculated using Multiwell code for the solution of the master equation of collisional energy transfer [17-18]. The microcanonical rate constants k(E) are calculated using the Rice-Ramsperger-Kassel-Markus (RRKM) expression. The collisional energy transfer probability was described by the exponential down model, with $\langle E_{down} \rangle$ = 260 cm^{-1} for argon [19]. Quantum tunneling was considered using the Eckart approach for reactions involving H-atom transfer [20-21]. Vibrational partition function, was calculated at the B3LYP/6-311G(d,p) level using the harmonic oscillator (HO) approximation, except for internal rotations of methyl groups. In these latter cases, a symmetric hindered rotor (HR) treatment was used following the methodology of Pitzer [22]. For cyclic transition states, the vibrational modes of the cyclic part of the molecular structure were described within the HO approximation, while the lateral methyl group internal rotations were treated as hindered rotors.

3. Results and discussion

3.1 Potential energy surface

All decomposition pathways of the initial adducts from H-atom addition on DMF were explored. A very large number of decomposition routes can be envisaged and the absence of rate rules and/or prior theoretical investigations precludes *a priori* eliminations of any decomposition channels. However, well-known principles of thermochemical kinetics should still apply: H-atom transfers through 3- and 4-

membered cyclic transition states are expected to be difficult. In the same way, C-H bond β-scissions can generally be neglected compared to C-C ones but can become competitive in the case of cyclic intermediates [23].

Figure 1 depicts the three possible initial steps for the DMF+H system, i.e., H-abstraction by H-atom from the methyl group, H-atom additions on the tertiary and secondary carbons as well as $R2C_6H_9O$ main decomposition route. Note that H-abstractions of hydrogen from the ring were not considered here because of very high bond dissociation energies [12].

The addition leading to resonantly stabilized $R1C_6H_9O$, is exothermic by -31.0 kcal mol^{-1} and has the lowest energy barrier (2.4 kcal mol^{-1}). The other addition yielding $R2C_6H_9O$ is less exothermic (-20.4 kcal mol^{-1}) and faces an higher critical energy of 3.7 kcal mol^{-1}. The H-abstraction pathway is also exothermic and has the highest computed energy barrier with a value of 5.9 kcal mol^{-1}. Table 1 presents comparisons of CBS-QB3, G4 and G3 critical energies. Computed G4 critical energies are found to be systematically lower than the G3 and CBS-QB3 values. The maximum deviation between the three methods (2.2 kcal mol^{-1}) is observed for the H-abstraction reaction. For the two additions the maximum deviation does not exceed 1.4 kcal mol^{-1}, which falls within the expected uncertainties of the three levels of theory. Results displayed in Table 1 allow us to estimate an uncertainty of ± 1.5 kcal mol^{-1} on the reaction energies and barriers computed at the CB3-QB3 level of theory. It should be noted that all transition states of reactions in Table 1, computed with the three composite methods, suffer from spin-contamination in the wave function based (post Hartree-Fock) calculation steps. The computed $<S^2>$ values are close to 1 instead of the expected value of 0.75. In CBS-QB3 and G4 methods, geometry optimizations are performed at the B3LYP level of theory and lead to optimized structures with almost no spin contamination. On the other hand, G3 geometries are optimized at the MP2 level of theory and may be less reliable because of spin-contaminated structures.

Figure 2 presents the CBS-QB3 and G4 H-abstraction rate coefficients along with the G3 value calculated by Simmie and Metcalfe [12]. Above 1000 K, a good agreement is observed between the three computed rate constants as the largest deviation lies within a factor of two. At 500 K, CBS-QB3 and G4 rates coefficients are in good agreement within a factor 1.5 while G3 value is lower by a factor of 3.0 and 4.5, respectively. These differences can mainly be ascribed to the variation in computed critical energies as shown in Table 1. Uncertainties are therefore larger at lowest temperatures, far from combustion and pyrolysis conditions. Note that quantum tunneling is not very important for this reaction. Calculated transmission coefficient is only 2.8 at 300 K, and decreases to 1.4 at 500 K reaching 1 near 700 K. The recommended modified Arrhenius expression for the H-abstraction reaction is $k_{CBS\text{-}QB3} = 1.54 \times 10^5 T^{2.7} \exp(-3434/RT)$ $cm^3.mol.s^{-1}$. The estimated uncertainty of the theoretical rate is around a factor 2 above 1000 K, and increases to a factor ~ 4 at 500 K.

From Figure 1, it can be seen that the most favored decomposition pathways of $R2C_6H_9O$ radical is the decomposition back to reactants with a barrier of 24.1 kcal mol^{-1}. H-atom shift to $R1C_6H_9O$ is shown to be unlikely to occur because of a high critical energy (39.9 kcal mol^{-1}). A similar activation energy of (39.2 kcal mol^{-1}) was reported at the G3 level of calculation for the C-H bond β-scission [12]. The barrier for the ring opening of $R2C_6H_9O$, leading to $R8C_6H_9O$, is lying above the entrance channel (13.1 kcal mol^{-1}) with a subsequent exit channel, leading to propyne and acetonyl radical, higher in energy. The dissociation back to DMF+H is expected to be the only important channel, and the formation of $R2C_6H_9O$ can be neglected. Preliminary master equation simulations concur with this conclusion.

$R1C_6H_9O$ is the only adduct playing a role in the addition of H-atom on DMF. A complete view of its decomposition pathways is critical to estimate the branching ratios of the products of the title reaction. This part of the text describes the efforts made to find exit channels that can compete with the ipso substitution (reaction R5).

Figure 3 presents five unimolecular reactions envisaged for R1C_6H_9O radical, involving one C-C bond breaking, one C-O bond breaking and three internal hydrogen transfer isomerizations. Computed energy barriers for the H-atom transfers are lying well above the entrance channel, by at least 20 kcal mol^{-1}. All the critical geometries for these processes involve strained bicyclic transition state as schematically shown on Figure 3. Moreover, these isomerizations are associated with a loss of the resonance energy. Note that a fourth H-atom shift, leading to R2C_6H_9O with a similar high-energy barrier, was already considered in Figure 1. The computed critical energy (31.2 kcal mol^{-1}) of the methyl group elimination from R1C_6H_9O is in very good agreement with the G3 value of 31.4 kcal mol^{-1} [12]. Calculated G4 barrier (31.9 kcal mol^{-1}) is also very close despite spin-contaminated wave functions at the three levels of theory. The other possible C-O bond β-scission leads to the opening of the ring with the lowest energy barrier, lying 7.5 kcal mol^{-1} below the entrance channel. The resonantly stabilized radical R3C_6H_9O formed is less stable than R1C_6H_9O only by 4.4 kcal mol^{-1} and constitute the starting intermediate towards exit channels that can compete with the ipso substitution.

Figure 4 depicts the computed PES describing subsequent decomposition routes of R3C_6H_9O. Five isomerization reactions and one C-C bond β-scission were considered. Once the ring is opened, C-C bond breaking leading to propenylketene and CH_3 constitutes an immediate exit channel. However, this β-scission features a high-energy barrier, lying 19.8 kcal mol^{-1} above the entrance channel. Note that this critical energy was not calculated here, but estimated by adding the activation energy of the addition of CH_3 on allenylketene from reference [12] to the reaction energy at 0 K of R3$C_6H_9O \rightarrow C_5H_6O+CH_3$. Again, strained transition state structures or loss of resonance stabilization energy lead to high-energy barrier. It is the case of H-atom shifts leading to R18C_6H_9O and R17C_6H_9O that can therefore be ignored. In agreement with thermochemical kinetics principles for alkanes isomerizations [24], five-, six- and seven-membered ring transition states are the most favored isomerization paths, leading to R7C_6H_9O, R5C_6H_9O and R4C_6H_9O, respectively. Note that, in these cases, resonantly stabilized

structures are conserved through the reactions. The energy barriers of H-atom shifts leading to R5C_6H_9O and R7C_6H_9O lie above the entrance channel by respectively 1.7 and 7.8 kcal mol^{-1}. Their decomposition paths were explored thoroughly and are described below (Figure 5 and 6). The lowest energy barrier of isomerization (5.9 kcal mol^{-1} below the entrance channel) gives R4C_6H_9O radical which contains an alcohol function formed via an internal H-abstraction by O atom. Exit channels, that can be reached from this intermediate, are presented on Figure 6.

The four decomposition routes considered for R5C_6H_9O are displayed on Figure 5. All these pathways feature bottlenecks with energies higher than the entrance channels. Similarly to R3C_6H_9O, C-C bond β-scission leading to ketene and a vinylic butenyl radical faces an important barrier of 45.5 kcal mol^{-1}. The three other routes explored involve successive rearrangements before reaching an exit channel. The path with the highest products channel involves first a H-shift to form R13C_6H_9O radical that can further give the very stable R16C_6H_9O (-30.7 kcal mol^{-1}) intermediate by ring closure. This ring enlargement (going from a C_5 ring in R3C_6H_9O to a C_6 ring) has a bottleneck slightly above the entrance channel (5.3 kcal mol^{-1}; R5$C_6H_9O \rightarrow$ R13C_6H_9O) but exit channels from R16C_6H_9O (C-H bond scission and ring opening followed by formaldehyde elimination) feature high-energy barriers. R17C_6H_9O formation, via a six-membered ring internal H-abstraction by O, is the decomposition pathway with the lowest energy (5.4 kcal mol^{-1}). R7C_6H_9O ring closure yields radical R24C_6H_9O, which can further eliminate a methyl to form 1,3cyclopentadien-1-ol with critical energies (relative to DMF+H) of 9.4 kcal mol^{-1} and 9.0 kcal mol^{-1}, respectively. The last path envisaged involves a ring closure yielding R15C_6H_9O followed by a ring opening to R21C_6H_9O that can eliminate CO by α-scission. The latter exit channel is the lowest one for all the DMF+H surface. However, the bottleneck of this path lies 13.2 kcal mol^{-1} above the entrance channel.

Figure 6 depicts computed decomposition routes of R4C_6H_9O and R7C_6H_9O radicals. Despite the large number of pathways explored, no exit channel below the entrance channel was identified. We

shall focus first on R7C_6H_9O that has two exit channels. The direct C-C bond β-scission yielding 1,3-butadiene and acetyl radical is characterized by a critical energy lying only 5.9 kcal mol^{-1} above the entrance channel. Note that R3C_6H_9O and R5C_6H_9O exhibit high-energy β-scission barriers (respectively 46.4 and 45.5 kcal mol^{-1}) compared to R7C_6H_9O (31.2 kcal mol-1). In the former cases, the formation of a ketene tends to increase the barrier height of the C-C β-scission. It is interesting to note that without any prior rearrangements, all radicals derived from DMF will therefore be difficult to decompose because of β-scissions involving ketene formation. Ring closure of R7C_6H_9O followed by the demethylation yielding 3-cyclopentenol can compete with the direct decomposition to 1,3-butadiene and CH_3CO as the exit channel can be reached with a critical energy lying 4.5 kcal mol^{-1} above the entrance channel.

Five decomposition routes were calculated for R4C_6H_9O radical. Two 6-membered ring H-shifts (leading to R20C_6H_9O and R13C_6H_9O) were computed with barriers (25.2 and 13.3 kcal mol^{-1} respectively) lying above the entrance channel. Formation of R20C_6H_9O is unfavorable because of the loss of resonant stabilization energy. R13C_6H_9O decomposition paths were discussed in Figure 5. Two other isomerizations paths via 5-membered (R11C_6H_9O) and 7-membered (R17C_6H_9O) ring transition states were determined. The strain in the 5-membered ring critical geometry lead to a high-energy barrier to form R11C_6H_9O (19.6 kcal mol^{-1} above DMF+H). Interestingly, ring closure of R11C_6H_9O further leads to 1,3cyclohexadien-1-ol, a phenol precursor under combustion conditions. Isomerization to R17C_6H_9O is the initial step towards the lowest energy decomposition route of R4C_6H_9O. With respect to the entrance channel, H-shift occurs with a barrier of 11.9 kcal mol^{-1} leading to R17C_6H_9O which ultimately decomposes to 1,3cyclopentadien-1-ol and CH_3 after ring closure as already detailed in Figure 5. The last pathway computed for R4C_6H_9O involves a direct ring closure to R6C_6H_9O (10.9 kcal mol^{-1}), followed by either OH or CH_3 elimination.

Decomposition routes of $R1C_6H_9O$ are shown to be rather complex. To determine which pathways are important for this system, we performed preliminary master equation calculations. All computed decomposition pathways of the chemically activated adduct $R1C_6H_9O$ with bottlenecks lying within 15 kcal mol^{-1} or less above the entrance channel were included in preliminary RRKM/ME simulations (using only HO approximation and with no tunneling). Temperature conditions from 500 K to 2000 K as well as pressures ranging from 0.01 to 100 bar were explored to determine the decomposition channels playing a role in the DMF + H addition reaction. The calculations showed that only two exit channels needed to be considered for the addition scheme: MF+CH_3 and 1,3-butadiene+CH_3CO. Note that 1,3-butadiene was detected in Lifshitz et al. in pyrolysis experiments. Under the broad range of conditions examined, all the other exit channels were found to be negligible.

3.1 Master equation modeling

The final RRKM/ME calculations were performed with three wells: $R1C_6H_9O$, $R3C_6H_9O$, and $R7C_6H_9O$, and three irreversible product channels: $C_6H_7O+H_2$ (direct abstraction), MF+CH_3 and 1,3-butadiene+CH_3CO. Lennard-Jones parameters for the three isomers were assumed equal to those of phenol [25]. Molecular and Lennard-Jones parameters are provided in the Supplemental Material section.

RRKM/ME modeling indicates that the total rate constant exhibits little to no pressure dependency, in agreement with the experiments. Figure 7 presents the rate constants computed at the high-pressure limit and in a 1 bar argon bath. The difference is very small on the 500–2000 K temperature range. The total rate constant at 1 bar is higher by a factor of two compared to the values calculated with the experimental Arrhenius expression. As the discrepancies observed falls within both experimental and theoretical uncertainty limits, no adjustment to the computed PES was performed. We recommend the following total computed rate constant:

$$k_{DMF+H \rightarrow products}\ (cm^3\ mol^{-1}\ s^{-1}) = 4.45 \times 10^5\ T^{2.538} e^{-599.3/T}$$

for $500 \leq T \leq 2000$ K with an uncertainty factor of 2.

At 500 K, hydrogen addition on DMF accounts for 96 % of the total rate constant. Under the experimental conditions of Friese et al. [13], H-abstraction by H-atom constitutes ~ 25% of the total rate. Figure 8 presents computed branching ratios at 1 bar. Below 900 K, stabilization of R1C_6H_9O and R3C_6H_9O is the dominant process. Note that R7C_6H_9O was never stabilized in our computations. Above 1000 K, the total rate constant is dominated by the H-abstraction reaction and the decomposition of the C_6H_9O isomers into MF+CH_3 and 1,3-C_4H_6+CH_3CO. As expected, the ipso substitution is predominant in the addition process. For the addition scheme alone (neglecting H-abstraction), it represents 45% yield at 1000 K increasing to 63% at 2000 K. The 1,3-C_4H_6+CH_3CO channel is also important above 1000 K. Focusing on the addition process only, it exhibits yields that increase rapidly from 900 to 1200 K (17 to 37 %) and slowly decrease towards higher temperature reaching a value of 26% at 2000 K. This behavior is explained by the dissociation of the addition products to reactants that compete with this channel above 1200 K.

Including the H-abstraction channel, the yields of MF+CH_3 and 1,3-C_4H_6+CH_3CO increase from the lowest temperatures and reach a maximum at 1100K (39 and 27 % respectively). Above 1100 K, the branching ratios of these two product channels decrease as H-abstraction channel starts to be dominant. ME/RRKM calculations showed that branching ratios of the DMF+H → products reaction are not very sensitive to pressure variations. At lowest pressures, the stabilization of C_6H_9O isomers becomes less important and the yields of MF+CH_3 and 1,3-C_4H_6+CH_3CO channels remain similar with maxima shifted towards lower temperatures. As expected, a similar effect is observed at higher pressures but with maxima displaced towards higher temperatures. The branching ratios of H-abstraction channel are found to be independent of pressure variations. Above 1500 K, master equation modeling showed that branching ratios are mostly pressure-independent.

Product yields were computed over the temperature range 500-2000 K, and pressure from 0.1 to 10 bar. Table 2 presents modified Arrhenius fits to the rate constants at 0.01, 0.1, 1, and 10 bar. They are provided for use in kinetic models.

4. Concluding remarks

The gas-phase reaction between 2,5-dimethylfuran and H-atom was investigated theoretically. The potential energy of the reaction was examined using the CBS-QB3 method. H-abstraction by H-atom as well as addition pathways were thoroughly explored. The calculated high-pressure limit rate constant for H-abstraction by H is in good agreement with literature G3 values under combustion conditions. A large number of decomposition pathways was envisaged for the C_6H_9O adducts. The total computed PES shows that among the complex interconnected pathways, the ipso substitution R5 is the only product channel with a bottleneck lying below the entrance channel. A few reaction paths were found to have energies lying slightly above the entrance channel. A preliminary master equation model was built including all channels with bottlenecks lying 15 kcal mol^{-1} above the entrance channel. It was shown that beside H-abstraction and ipso substitution channels, the product channel yielding 1,3-butadiene and acetyl radical is important. All other channels can be neglected. RRKM/master equation modeling, based on the simplified PES, was carried out to determine the branching ratios to a wide ranges of pressure and temperature.

The total rate constant was also found in good agreement with Friese et al. experimental data. Moreover, the total rate constant was computed to be nearly independent of pressure, in agreement with the experiments. Under high-temperature combustion conditions, the three product channels are dominant. At 1100 K and 1 bar, the branching ratios of the product channels from the addition process MF+CH_3 and 1,3-butadiene+CH_3CO are maximal. Above 1100 K the yields of these two exit channels

decrease slowly as the H-abstraction becomes dominant. Therefore, the fate of C_6H_7O radical is expected to be critical in the combustion chemistry of DMF.

On the basis of the computed branching ratios, pressure-dependent rate expressions are proposed for the title reaction over the temperature and pressure ranges of interest to combustion modeling.

Acknowledgements

This work was granted access to the HPC resources of CINES under the allocation 2011086686 made by GENCI. This study was supported by the European Commission through the “Clean ICE” Advanced Research Grant of the European Research Council.

References

[1] L. Sy Tran, B. Sirjean, P.A. Glaude, R. Fournet, F. Battin-Leclerc, Energy, in press (2011).
[2] Y. Román-Leshkov, C.J. Barrett, Z.Y. Liu, J.A. Dumesic, Nature, 447 (2007) 982-985.
[3] H. Zhao, J.E. Holladay, H. Brown, Z.C. Zhang, Science, 316 (2007) 1597-1600.
[4] R. Daniel, G. Tian, H. Xu, M.L. Wyszynski, X. Wu, Z. Huang, Fuel, 90 (2011) 449-458.
[5] S. Zhong, R. Daniel, H. Xu, J. Zhang, D. Turner, M.L. Wyszynski, P. Richards, Energ. Fuel, 24 (2010) 2891-2899.
[6] G. Tian, R. Daniel, H. Li, H. Xu, S. Shuai, P. Richards, Energ. Fuel, 24 (2010) 3898-3905.
[7] X. Wu, Z. Huang, X. Wang, C. Jin, C. Tang, L. Wei, C.K. Law, Combust. Flame, 158 (2011) 539-546.
[8] F. Battin-Leclerc, E. Blurock, R. Bounaceur, R. Fournet, P.A. Glaude, O. Herbinet, B. Sirjean, V. Warth, Chem. Soc. Rev., 40 (2011) 4762-4782.
[9] M.A. Grela, V.T. Amorebieta, A.J. Colussi, J. Phys. Chem., 89 (1985) 38-41.
[10] A. Lifshitz, C. Tamburu, R. Shashua, J. Phys. Chem. A, 102 (1998) 10655-10670.
[11] X. Wu, Z. Huang, T. Yuan, K. Zhang, L. Wei, Combust. Flame, 156 (2009) 1365-1376.
[12] J.M. Simmie, W.K. Metcalfe, J. Phys. Chem. A, 115 (2011) 8877-8888.
[13] P. Friese, T. Bentz, M. Olzmann, J.M. Simmie, Proceedings of the European Combustion Meeting, 2011, Cardiff, Wales, June 29 - July 1st 2011, (2011).
[14] M.J. Frisch, G.W. Trucks, H.B. Schlegel, G.E. Scuseria, M.A. Robb, J.R. Cheeseman, G. Scalmani, V. Barone, B. Mennucci, G.A. Petersson, H. Nakatsuji, M. Caricato, X. Li, H.P. Hratchian, A.F. Izmaylov, J. Bloino, G. Zheng, J.L. Sonnenberg, M. Hada, M. Ehara, K. Toyota, R. Fukuda, J. Hasegawa, M. Ishida, T. Nakajima, Y. Honda, O. Kitao, H. Nakai, T. Vreven, J.A. Montgomery, J.E. Peralta, F. Ogliaro, M. Bearpark, J.J. Heyd, E. Brothers, K.N. Kudin, V.N. Staroverov, R. Kobayashi, J. Normand, K. Raghavachari, A. Rendell, J.C. Burant, S.S. Iyengar, J. Tomasi, M. Cossi, N. Rega, J.M. Millam, M. Klene, J.E. Knox, J.B. Cross, V. Bakken, C. Adamo, J. Jaramillo, R. Gomperts, R.E. Stratmann, O. Yazyev, A.J. Austin, R. Cammi, C. Pomelli, J.W. Ochterski, R.L. Martin, K. Morokuma, V.G. Zakrzewski, G.A. Voth, P. Salvador, J.J. Dannenberg, S. Dapprich, A.D. Daniels, Farkas, J.B. Foresman, J.V. Ortiz, J. Cioslowski, D.J. Fox, in Wallingford CT, 2009.
[15] J.A. Montgomery, M.J. Frisch, J.W. Ochterski, G.A. Petersson, J. Chem. Phys., 110 (1999) 2822-2827.
[16] L.A. Curtiss, P.C. Redfern, K. Raghavachari, J. Chem. Phys., 126 (2007).
[17] J.R. Barker, N.F. Ortiz, J.M. Preses, L.L. Lohr, A. Maranzana, P.J. Stimac, T.L. Nguyen, T.J.D. Kumar, in, University of Michigan, Ann Arbor, MI; http://aoss.engin.umich.edu/multiwell/, 2011.
[18] J.R. Barker, Int. J. Chem. Kinet., 33 (2001) 232-245.
[19] A.V. Joshi, H. Wang, Int. J. Chem. Kinet., 38 (2006) 57-73.
[20] C. Eckart, Phys. Rev., 35 (1930) 1303-1309.
[21] J.A. Miller, J. Am. Chem. Soc., 101 (1979) 6810-6814.
[22] K.S. Pitzer, J. Chem. Phys., 12 (1944) 310-314.
[23] B. Sirjean, P.A. Glaude, M.F. Ruiz-Lopèz, R. Fournet, J. Phys. Chem. A, 112 (2008) 11598-11610.
[24] B. Sirjean, E. Dames, H. Wang, W. Tsang, J. Phys. Chem. A, 116 (2012) 319-332.
[25] C.A. Taatjes, D.L. Osborn, T.M. Selby, G. Meloni, A.J. Trevitt, E. Epifanovsky, A.I. Krylov, B. Sirjean, E. Dames, H. Wang, J. Phys. Chem. A, 114 (2010) 3355-3370.

Table 1. Critical energies (kcal mol^{-1}) computed for initial DMF + H reaction steps at 0K.

	CBS-QB3[a]	G4[a]	G3[12]
DMF + H ⇆ R1C_6H_9O	2.4	1.0	1.8
DMF + H ⇆ R2C_6H_9O	3.7	2.7	3.8
DMF + H → C_6H_7O + H_2	5.9	4.9	7.1

[a] This work.

Table 2. Monte Carlo RRKM/master equation results fitted to modified Arrhenius expressions.[a]

		$k(T) = A\,T^n\,e^{-B/T}$			
Reaction channel	P (bar)	A	n	B	T (K)
DMF + H → C_6H_7O + H_2		1.54×10^{5}	2.70	3434	300-2000
DMF + H → MF + CH_3	0.01	5.82×10^{19}	–1.61	4862	500-2000
	0.1	4.59×10^{22}	–2.39	6228	500-2000
	1	2.32×10^{22}	–2.27	6651	500-2000
	10	5.86×10^{25}	–3.18	8415	500-2000
DMF + H → 1,3-C_4H_6 + CH_3CO	0.01	1.34×10^{32}	–5.24	8558	500-2000
	0.1	7.21×10^{41}	–7.93	12481	500-2000
	1	1.72×10^{53}	–11.04	17636	500-2000
	10	2.85×10^{67}	–14.87	24861	600-2000
DMF + H → R1C_6H_9O	0.01	8.45×10^{64}	–17.52	8321	500-900
	0.1	2.92×10^{30}	–7.01	17	500-1000
	1	1.11×10^{45}	–11.17	3123	500-1500
	10	5.77×10^{88}	–24.02	13317	500-1500
DMF + H → R3C_6H_9O	0.01	2.29×10^{202}	–58.90	35975	500-1000
	0.1	2.51×10^{167}	–47.59	30961	500-1100
	1	7.72×10^{103}	–27.53	20535	500-1500
	10	5.26×10^{143}	–39.13	31441	500-1500

[a] Units are $cm^3mole^{-1}s^{-1}$ and K. Rates computed with argon as the bath gas.

Figure Captions:

Figure 1. Potential energy surface of initial additions and abstraction steps of DMF + H system and decomposition pathway of adduct R2C_6H_9O computed using the CBS-QB3 method at 0 K. Dashed line: G3 energy barrier from [12].

Figure 2. Arrhenius plots of H-abstraction reaction DMF + H → C_6H_7O + H_2 (see Figure 1 for C6H7O structure). Dotted line: G3 calculation from Simmie and Metcalfe [12].

Figure 3. Potential energy surface of initial decomposition pathways of adduct R1C_6H_9O computed using the CBS-QB3 method at 0 K.

Figure 4. Potential energy surface of decomposition pathways of R3C_6H_9O computed using the CBS-QB3 method at 0 K. Dashed line: barrier taken from calculations of reference [12] (see text).

Figure 5. Potential energy surface of decomposition pathways of R5C_6H_9O computed at the CBS-QB3 level of theory at 0 K. Potential energy relative to the entrance channel DMF + H.

Figure 6. Potential energy surface of the decomposition pathways of R7C_6H_9O and R4C_6H_9O computed at the CBS-QB3 level of theory at 0 K. Potential energy relative to the entrance channel DMF + H.

Figure 7. Arrhenius plot for of the total rate constant of reaction DMF + H → products. Symbols represent experimental data from [13].

Figure 8. Product branching ratios of the DMF + H → products reaction at 1 bar of Ar bath gas.

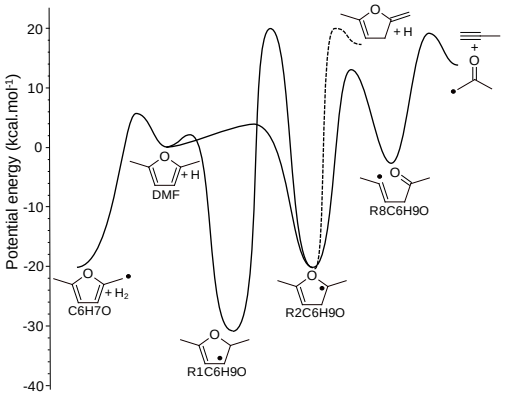

Figure 1. Potential energy surface of initial additions and abstraction steps of DMF + H system and decomposition pathway of adduct $R2C_6H_9O$ computed using the CBS-QB3 method at 0 K. Dashed line: G3 energy barrier from [12].

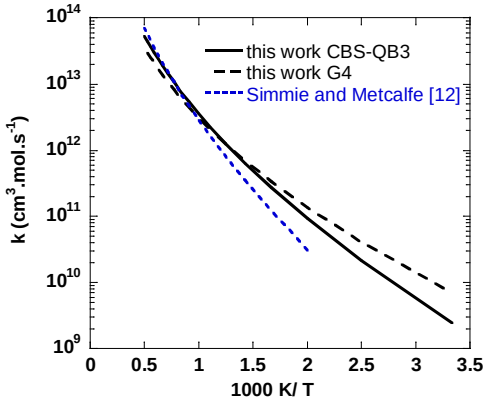

Figure 2. Arrhenius plots of H-abstraction reaction DMF + H → C_6H_7O + H_2 (see Figure 1 for C_6H_7O structure). Dotted line: G3 calculation from Simmie and Metcalfe [12].

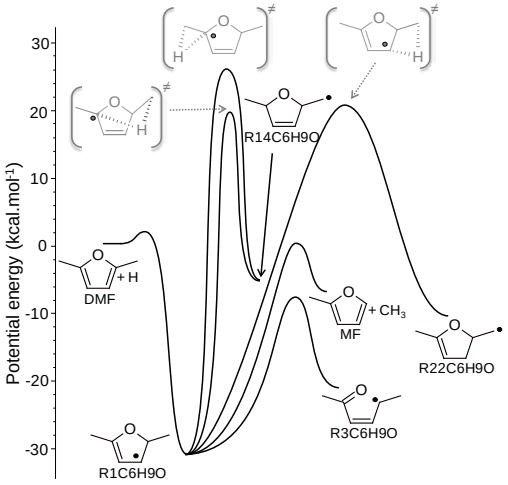

Figure 3. Potential energy surface of initial decomposition pathways of adduct $R1C_6H_9O$ computed using the CBS-QB3 method at 0 K.

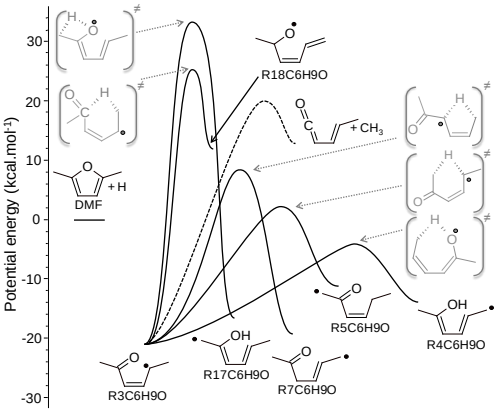

Figure 4. Potential energy surface of decomposition pathways of $R3C_6H_9O$ computed using the CBS-QB3 method at 0 K. Dashed line: barrier taken from calculations of reference [12] (see text).

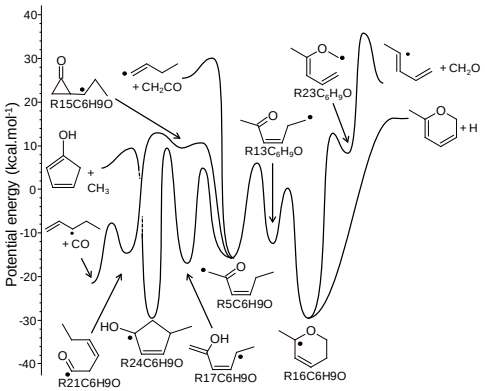

Figure 5. Potential energy surface of decomposition pathways of $R5C_6H_9O$ computed at the CBS-QB3 level of theory at 0 K. Potential energy relative to the entrance channel DMF + H.

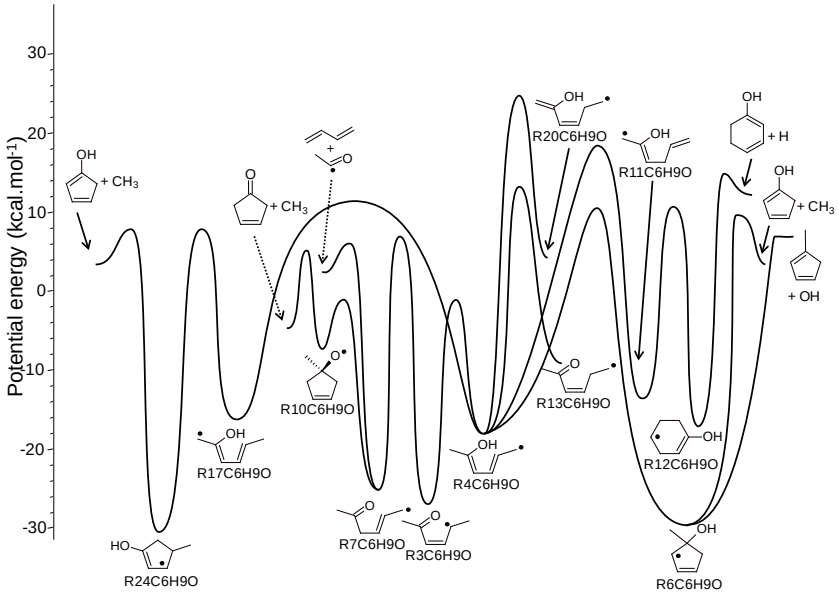

Figure 6. Potential energy surface of the decomposition pathways of $R7C_6H_9O$ and $R4C_6H_9O$ computed at the CBS-QB3 level of theory at 0 K. Potential energy relative to the entrance channel DMF + H.

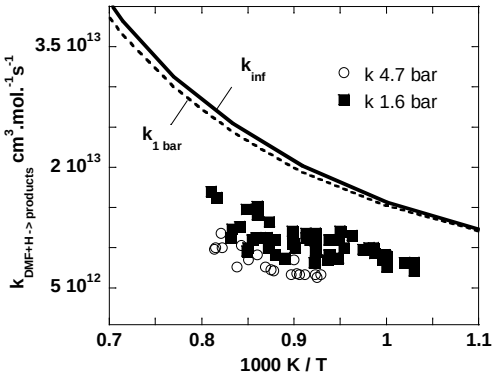

Figure 7. Arrhenius plot for of the total rate constant of reaction DMF + H→ products. Symbols represent experimental data from [13].

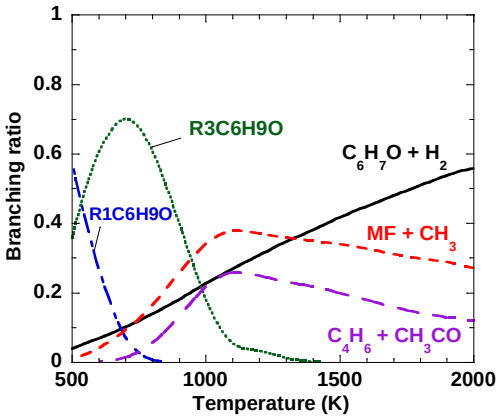

Figure 8. Product branching ratios of the DMF + H → products reaction at 1 bar of Ar bath gas.

Supplemental material:

Table S1: Molecular and Lennard-Jones parameters used in RRKM/ME calcuations.

Table S2: Optimized geometries in cartesian coordinates.

Table S3: Electronic energies computed at the CBS-QB3 level of theory (Hartree, 0 K).

Table S4: Isodesmic reactions used to compute the enthalpies of formation.